The Journal of Immunology

Injury-Induced Type I IFN Signaling Regulates Inflammatory Responses in the Central Nervous System

Reza Khorooshi and Trevor Owens

J Immunol 2010; 185:1258-1264; Prepublished online 18 June 2010;
doi: 10.4049/jimmunol.0901753
http://www.jimmunol.org/content/185/2/1258

The Journal of Immunology is published twice each month by
The American Association of Immunologists, Inc.,
1451 Rockville Pike, Suite 650, Rockville, MD 20852

Print ISSN: 0022-1767 Online ISSN: 1550-6606.

Injury-Induced Type I IFN Signaling Regulates Inflammatory Responses in the Central Nervous System

Reza Khorooshi and Trevor Owens

Innate glial response is critical for the induction of inflammatory mediators and recruitment of leukocytes to sites of the injury in the CNS. We have examined the involvement of type I IFN signaling in the mouse hippocampus following sterile injury (transection of entorhinal afferents). Type I IFNs signal through a receptor (IFNAR), which involves activation of IFN regulatory factor (IRF)9, leading to the induction of IFN-stimulated genes including *IRF7*, that in turn enhances the induction of type I IFN. Axonal transection induced upregulation of *IRF7* and *IRF9* in hippocampus. Induction of *IRF7* and *IRF9* mRNAs was IFNAR dependent. Double-labeling immunofluorescence showed that IRF7 selectively was induced in Mac-1/CD11b$^+$ macrophages/microglia in hippocampus after axonal transection. *IRF7* mRNA was also detected in microglia sorted by flow cytometry. Lack of type I IFN signaling resulted in increased leukocyte infiltration into the lesion-reactive hippocampus. Axonal lesion-induced *CXCL10* gene expression was abrogated, whereas *matrix metalloproteinase 9* mRNA was elevated in IFNAR-deficient mice. Our findings point to a role for type I IFN signaling in regulation of CNS response to sterile injury. *The Journal of Immunology*, 2010, 185: 1258–1264.

Injury to the CNS induces an innate glial response, in which microglia and astrocytes become activated. This response is essential for the induction of cytokines and chemokines, which initiate a variety of cellular responses including the migration of peripheral immune cells into the damaged tissue. The activation of glial cells and the entry of leukocytes may be beneficial for repair and regeneration processes in the damaged CNS but may also exacerbate neurodegeneration (1, 2).

The molecular basis for glial activation is poorly understood. The initial glial response involves TLR signaling, which can induce proinflammatory cytokines (3, 4), among them type I IFNs. Type I IFNs (IFN-α and IFN-β) play a critical role in the innate immune response against viral infection (5). The signaling pathway for both IFN-α and IFN-β involves a common cell surface receptor, IFNAR. IFNAR is associated with STAT1 and STAT2, which together with IFN regulatory factor (IRF)9 form a complex that binds to IFN-stimulated response element in promotor regions and stimulates type I IFN-dependent gene transcription including *IRF7* (6, 7). *IRF7* has been described as a master regulator of type I IFN signaling (8, 9).

Type I IFN signaling is normally associated with antiviral immune responses (10). IFN-β is also used in the treatment of multiple sclerosis, and mice with defective type I IFN signaling develop more severe experimental autoimmune encephalomyelitis (EAE) (11, 12), indicating the involvement of type I IFN signaling in the regulation of CNS inflammation. Involvement of type I IFN in a noninfectious injury-induced glial response has not been studied. A well-established and widely used model to study the glial response after brain injury is an entorhinal axonal lesion. The transection of projections from entorhinal cortex to the hippocampus leads to anterograde axonal degeneration and loss of synapses in the outer molecular layer of the dentate gyrus, followed by glial activation, leukocyte infiltration, and sprouting (13–20). Involvement of TLR signaling as well as cytokines (TNF-α and IL-1β) and chemokines (CCL2 and CXCL10) in glial response and recruitment of leukocytes in the lesion-reactive hippocampus have been described previously (15, 17, 21, 22). We previously described glial upregulation of STAT1 and STAT2 (21), which suggested the involvement of type I IFN signaling.

The aim of this study was to examine the involvement and functional significance of type I IFN signaling in lesion-induced glial responses. We show that sterile axonal lesion induces *IRF7* and *IRF9* gene expression and that this is IFNAR dependent. Immunohistochemical staining and flow cytometry localized IRF7 to Mac1/CD11b$^+$ macrophages/microglia in lesion-reactive hippocampus at 1 d postlesion. Leukocyte infiltration was increased in IFNAR-deficient mice. Unlike wild-type (WT) mice, axonal lesion did not induce an increase in *CXCL10*, but it induced an increase in matrix metalloproteinase (*MMP*)*9* gene expression in IFNAR-knockout (KO) mice. These findings identify a role for type I IFN in regulating innate responses to CNS injury.

Materials and Methods

Animals

Adult female mice deficient in STAT1 (STAT1-KO) 129s6/SvEv background (23) were purchased from Taconic Farms (Germantown, NY), IFNAR-KO on 129s6/SvEv background were purchased from B&K Universal Limited (Hull, U.K.), IRF7-KO on C57BL/6 background were purchased from Riken BRC (Tsukuba, Japan) with agreement from Dr. T. Taniguchi (Department of Immunology, University of Tokyo, Tokyo, Japan) (9), and IFNAR-KO on C57BL/6 background (11) were provided by Dr. M. Prinz (Department of Neuropathology, University of Freiburg, Germany). WT mice (C57BL/6 and129s6/SvEv) were purchased from Taconic (Taconic Europe, Ry, Denmark). These experiments were conducted according to the guidelines of the National Danish Animal Research Committee.

Entorhinal cortex lesioning and tissue preparation

Under anesthesia, adult female (18–20 g) mice were placed in a Kopf stereotactic apparatus (Kopf Instruments, Tujunga, CA). The entorhino-

Institute of Molecular Medicine, University of Southern Denmark, Odense, Denmark

Received for publication June 3, 2009. Accepted for publication May 11, 2010.

This work was supported by grants from the Danish Agency for Science, Technology, and Innovation; Novo Nordisk Fonden; Lundbeckfonden; Augustinus Fonden; and Aase and Ejnar Danielsens Fond.

Address correspondence and reprint requests to Dr. Trevor Owens, Institute of Molecular Medicine, University of Southern Denmark, J.B. Winsloewsvej 25, 5000 Odense C, Denmark. E-mail address: towens@health.sdu.dk

Abbreviations used in this paper: C, contralateral; DG, dentate gyrus; dpl, day postlesion; EAE, experimental autoimmune encephalomyelitis; FJ, Fluoro-Jade; IRF, IFN regulatory factor; KO, knockout; L, lesion-reactive hippocampi; *MMP*, matrix metalloproteinase; OML, outer molecular layer; WT, wild-type.

www.jimmunol.org/cgi/doi/10.4049/jimmunol.0901753

dentate perforant path projection was transected as described previously (21).

For immunohistochemical analysis, mice were perfused transcardially with PBS, followed by 4% paraformaldehyde (Sigma-Aldrich, Broendby, Denmark) in PBS. The brains were removed and postfixed in PBS containing 4% paraformaldehyde for 2 h on ice, then immersed in 30% sucrose in PBS overnight at 4°C, frozen with CO_2-snow, and stored at −20°C until sectioning. For flow cytometry and quantitative real-time RT-PCR analysis, mice were perfused transcardially with PBS, and brains were removed aseptically.

Single- and dual-labeling immunohistochemistry

Immunohistochemical staining was performed as described previously (21). In brief, after blocking endogenous peroxidases, the sections were incubated overnight with rabbit anti-IRF7 Ab (SC-9083; Santa Cruz Biotechnology, Santa Cruz, CA), rat anti-mouse Mac-1/CD11b (MCA711; Serotec, Oxford, U.K.) (to identify microglia/macrophages), or rabbit anti-GFAP (Z0334; DakoCytomation, Glostrup, Denmark) (to identify astrocytes), and in the following day, the sections were incubated with secondary biotinylated Ab (Amersham Biosciences, Little Chalfont, U.K.). The sections were finally incubated with streptavidin-HRP (P0397; DakoCytomation) and developed with 0.5 mg/ml diaminobenzidine (Sigma-Aldrich).

For dual-labeling immunofluorescence, sections were incubated with rabbit anti-IRF7 and with rat anti-mouse Mac-1/CD11b or monoclonal mouse anti–GFAP-cy3–conjugated Abs (C9205; Sigma-Aldrich), followed by incubation with fluorescent secondary Abs, Alexa 488-labeled goat anti-rabbit (A11034; Invitrogen, Taastrup, Denmark) and Alexa 568-labeled goat anti-rat (A11077; Invitrogen), as described previously (21). Images were acquired using either an Olympus BX51 microscope (Olympus, Ballerup, Denmark) connected to an Olympus DP71 digital camera and a Confocal laser scanning fluorescence microscope (Olympus FV1000; Olympus, Hamburg, Germany). Images were combined using Adobe Photoshop CS version 8.0 to visualize double-labeled cells. To verify Ab specificity, control sections were treated without primary Ab or with isotype-matched primary Abs. Control sections displayed no staining comparable with that seen with primary Abs (data not shown).

Western blotting

Western blot analysis was performed as described previously (21). Both contralateral and ipsilateral hippocampi were isolated from PBS-perfused mice and lysed in lysis buffer. Cell lysate was mixed with sample buffer, denatured by boiling, and separated by electrophoresis in an 8–10% polyacrylamide gel. The separated proteins were transferred to a nitrocellulose membrane (Bio-Rad, Hercules, CA). The membranes were blocked for 1 h at room temperature in 5% nonfat dry milk in PBS containing 0.1% Tween 20 (PBST). The membranes were then incubated with rabbit anti-IRF7 and/or rabbit anti-actin (A5060; Sigma-Aldrich) Abs at 4°C overnight. After washing in PBST, the membranes were incubated with goat anti-rabbit IgG HRP conjugate (Sigma-Aldrich) for 1 h at room temperature. Staining was detected using chemical luminescence methodology (GE Healthcare U.K., Amersham Place, U.K.). The intensities of IRF7 and actin were calculated using an image analyzing system (ImageJ; National Institutes of Health, Bethesda, MD). The relative levels of IRF7 were normalized against the levels of actin, and values from lesion-reactive hippocampi were divided by the values from contralateral to calculate the fold induction of IRF7.

Fluoro-Jade staining

Fluoro-Jade (FJ) is used as a marker to identify degenerating neuronal tissue (24). To examine whether lack of IFNAR signaling may affect FJ staining in the outer molecular layer of dentate gyrus, brain sections were stained with FJ (Histo-Chem, Jefferson, AK). Sections were immersed in 100% ethanol for 3 min in 70% ethanol for 1 min and rinsed in H_2O for 1 min before being incubated for 15 min in 0.06% $KMnO_4$. Thereafter, tissue was rinsed for 1 min in H_2O and stained for 45 min in 0.001% FJ solution diluted in 0.1% acetic acid. Sections were then rinsed in distilled water, air-dried, dipped in xylene, coverslipped, and mounted with Depex.

Quantitative real-time PCR

As previously described (21), RNA was isolated from the contralateral, ipsilateral, and unmanipulated hippocampi and converted to cDNA. Quantitative real-time PCR was performed using an ABI Prism 7300 Sequence Detection System (Applied Biosystems, Foster City, CA) (21). 18S rRNA was measured as a control and used to normalize gene expression (Applied Biosystems). Primer and probe sequences were as follows: CCL2 (forward, TCT GGG CCT GCT GTT CAC A; reverse, CCTACTCATTGGGATCATCTTGCT; probe, FAM-CTCAGCCAGATGCAGTT-MGB); TNF-α (forward, CCAAATGGCCTC CCTCTCAT; reverse, TCCTCCACTTGGTGGTTTGC; probe, FAM-CTCACACTCAGATCAT-MGB); *CXCL10* (forward, GCCGTCATT TTCTGCCTCAT; reverse, GGCCCGTCATCGATA TGG; probe, FAM-GGACTCAAGGGATCC-MGB); IL-1β (forward, CTTGGGCCTCAAAGG AAAGAA; reverse, AAGACAAACCGTTTTTCCATCTTC; probe, FAM-AGC TGG AGAGTGTGGAT-MGB); *IRF7* (forward, CACCCCCATCTTCGACTTCA; reverse, CCAAAACCCAGGTAGATGGTGTA; probe, FAM-CACTTTCTTCCGAGAACT-MGB); *IRF9* (forward, ACAACTGAGGCCACCATTAGAGA; reverse, CACCACTCGGCCACCATAG; probe, FAM-TGAACTCAGACTACTCGCT-MGB); *IRF3* (forward, CACCCCAAGAAAATCCACTGA; reverse, AGGCGGTCACCTCGAACTC; probe, FAM-TAGCTGAGGAACAATG-MGB); and *MMP9* (forward, CGAACTTCGACACTGACAAGAAGT; reverse, GCACGCTGGAATGATCTAAGC; probe, FAM-TCTGTCCAGACCAAGGGTACAGCCTGTTC-MGB).

Flow cytometry

To measure leukocyte entry in response to axonal injury, hippocampi were homogenized and incubated with blocking solution to block nonspecific staining as described previously (21). Cells were then stained with rat anti-mouse CD45-conjugated PE, rat anti-CD11b–conjugated PerCP, and hamster anti-mouse TCR-β–conjugated APC Abs (BD Biosciences, Erembodegem, Belgium) to detect microglia/macrophages or T cells, respectively (15, 17). Data were collected on a FACSCalibur (BD Biosciences, San Jose, CA) and analyzed using FlowJo software (Tree Star, Ashland, OR) (21).

To sort microglia and macrophages, hippocampi were pooled from six mice, and a similar experiment was performed as described above with few modifications. Homogenates were enriched for mononuclear cells by centrifugation through 33% isotonic Percoll prior to blocking the nonspecific staining. After staining with respective Abs, cells were sorted by a FACSVantage/Diva Sorting Flow Cytometer (BD Biosciences). Total RNA was extracted using TRIzol reagent as previously described (21) and converted to cDNA, and quantitative real-time PCR was performed as described above. ΔCT values for *IRF7* gene expression were then calculated. ΔCT is the difference in CT between *IRF7* gene and the internal reference control gene, 18S rRNA.

Data analysis

Results were analyzed by two-tailed paired/unpaired *t* test or one-way ANOVA with Bonferroni's posttest using GraphPad Prism software (GraphPad Software, San Diego, CA). A value of $p < 0.05$ was considered to be statistically significant. Data are presented as mean ± SEM.

Results

Lesion-induced IRF7 *gene expression was STAT1 and IFNAR dependent*

IRF7 mRNA was constitutively expressed at low levels in unmanipulated hippocampi from WT, IFNAR-KO, and STAT1-KO mice (data not shown). Levels of *IRF7* increased significantly in lesion-reactive hippocampi of WT mice at 1, 3, and 5 d (Fig. 1*A*). In contrast, axonal lesion did not induce a significant increase in *IRF7* gene expression in IFNAR-KO and STAT1-KO mice (Fig. 1*A*). Whether or not mice were on 129s6/SvEv (Fig. 1*A*) or C57BL/6 (Fig. 1*B*) background had no effect on these events.

Like *IRF7*, *IRF9* mRNA was constitutively expressed at low levels in unmanipulated hippocampi from both WT and IFNAR-KO mice (data not shown). *IRF9* mRNA levels increased in the lesion-reactive hippocampi at 1 d postlesion, and this was also IFNAR dependent (Fig.1*C*).

In addition to *IRF7* and *IRF9*, we also examined *IRF3* gene expression. *IRF3* is involved in the early induction of type I IFNs in antiviral immune response (25). *IRF3* was constitutively expressed in unmanpulated hippocampi in both WT and IFNAR-KO mice. Unlike *IRF7* and *IRF9*, there was no induction of *IRF3* at 1 d after lesion (data not shown).

IRF7 *was expressed by microglia/macrophages in the outer molecular layer of dentate gyrus*

We next examined IRF7 distribution and cellular localization in the denervated outer molecular layer of the dentate gyrus at 1 d postlesion. IRF7 immunoreactivity was not evident in unmanipulated

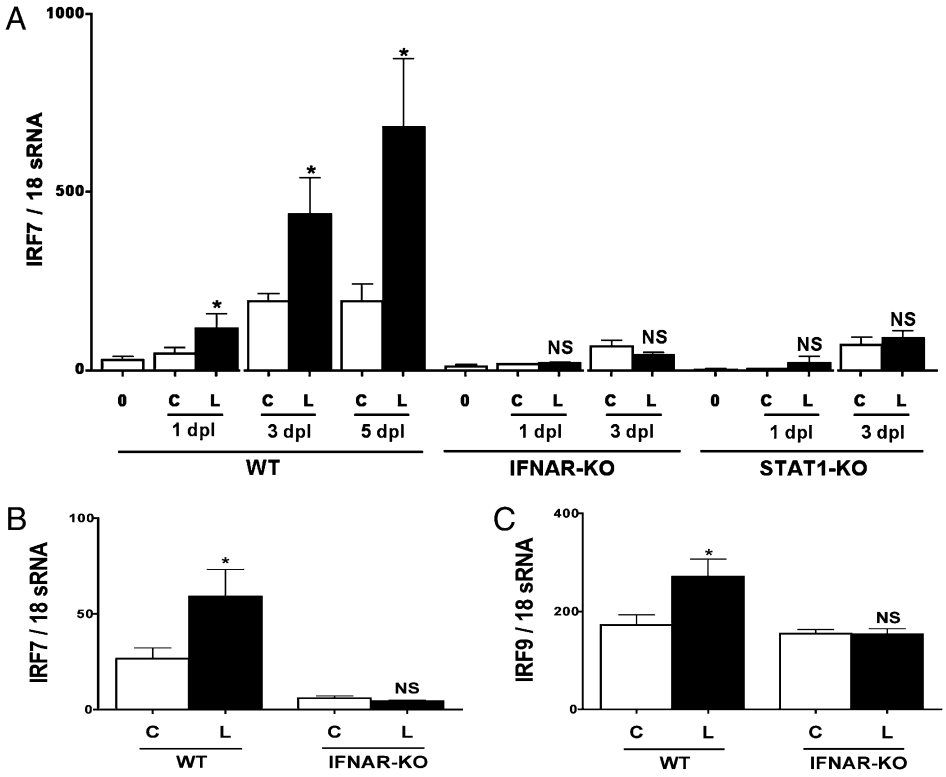

FIGURE 1. Injury-induced increase in *IRF7* and *IRF9* gene expression was IFNAR and STAT1 dependent. *A*, *IRF7* mRNA increased significantly in lesion-reactive hippocampi of 129s6/SvEv WT but not in IFNAR-KO and STAT1-KO mice at 1, 3, and 5 d postaxonal lesion. *B*, *IRF7* mRNA increased significantly in lesion-reactive hippocampi of C57BL/6 WT but not in IFNAR-KO mice on C57BL/6 background. *C*, *IRF9* gene expression was increased in lesion-reactive hippocampi of WT but not in IFNAR-KO mice at 1 d postlesion. Groups of matched contralateral and lesion-reactive hippocampi were analyzed by two-tailed paired Student *t* test. ∗Statistically significant differences versus contralateral as follows: *A*, 1 day postlesion (dpl), $p = 0.009$; 3 dpl, $p = 0.031$; 5 dpl, $p = 0.031$; *B*, WT, $p = 0.0039$; and *C*, WT, $p = 0.001$. Error bars represent SEM. C, contralateral; L, lesion-reactive hippocampi.

hippocampus and in corresponding regions of the contralateral hippocampus in lesioned animals (Fig. 2*A*). However, axonal lesion-induced increased IRF7 immunostaining in the outer molecular layer in dispersed cells that had morphologic features resembling activated microglia or macrophages (Fig. 2*B*, 2*C*). Double labeling with Mac-1/CD11b and GFAP showed that IRF7 colocalized with Mac-1/CD11b (Fig. 2*D–G*) and not with GFAP (Fig. 2*H–K*), indicating expression in microglia/macrophages.

IRF7 protein was also detected by Western blotting (data not shown). We identified relevant bands on the basis of their absence from Western blots of hippocampal lysates from IRF7-KO mice; this verified the specificity of IRF7 Ab (data not shown). The level of IRF7 protein did not increase at 1 d postlesion in lesion-reactive hippocampi compared with contralateral from either WT or IFNAR-KO mice (data not shown).

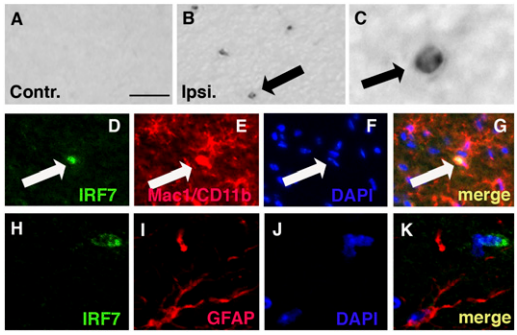

FIGURE 2. IRF7 immunoreactivity increased in lesion-reactive hippocampi at 1 d postlesion. *A*, IRF7 immunoreactivity was not evident in contralateral hippocampus. *B*, Axonal lesion-induced increase IRF7 immunoreactivity was detected in a few cells (arrow) dispersed within denervated outer molecular layer. *C*, Higher magnification of IRF7 immunoreactive cells (arrow) in *B*. *D–K*, Double labeling of IRF7 with Mac-1/CD11b (*D–G*) and GFAP (*H–K*) Abs showed that IRF7 immunoreactivity colocalized with Mac-1/CD11b-immunoreactive cells (*D–G*, arrow) but not with GFAP-immunostained cells (*H–K*). C, contralateral; L, lesion-reactive hippocampi. Original magnification ×20 (*A*, *B*, *H–K*), ×40 (*C*, *D–G*). Scale bars, 25 μm (*A*, *B*); 10 μm (*C*); 50 μm (*D–G*); and 20 μm (*H–K*).

IRF7 *gene expression in sorted CD45^{dim}CD11b^{+} microglia*

The expression of IRF7 protein in Mac-1/CD11b microglia/macrophages was confirmed by analysis of *IRF7* gene expression in microglia sorted by flow cytometry (Fig. 3). *IRF7* gene expression could be detected in sorted CD45^{dim}CD11b^{+} microglia at 1 d postaxonal lesion (Fig. 3). ΔCT values for *IRF7* gene expression in CD45^{dim}Cd11b^{+} microglia were ~16 (Fig. 3*B*). Because of the limited number of CD45^{high} CD11b macrophages sorted by flow cytometry from hippocampi, we were not able to detect *IRF7* gene expression in macrophages (Fig. 3).

Lesion-induced leukocyte infiltration was increased in IFNAR-KO mice

The upregulation of downstream components of type I IFN signaling indicates involvement in axonal lesion-induced glial response. Low levels of type I IFN gene expression could be detected in hippocampal samples by quantitative real-time PCR (data not shown). However, expression was difficult to detect, and it was not possible to reliably determine whether axonal-lesion influenced type I IFN induction, consistent with findings by Ousman et al. (10), in which the levels of type I IFN within the CNS were at the limit of detection even after several days postvirus infection.

To examine the functional significance of type I signaling in this model, leukocyte recruitment to the lesion-reactive hippocampi was analyzed by flow cytometry, measuring the proportion of CD45^{high} cells (Fig. 4*A*). Proportions of blood-derived leukocytes were similarly low in unmanipulated hippocampi from WT and IFNAR-KO mice, regardless of strain background. The proportion of CD45 ^{high} cells was significantly increased in lesion-reactive hippocampi of both WT and IFNAR-KO mice compared with the contralateral hippocampus of each mouse, regardless of whether WT and IFNAR-KO mice were on C57BL/6 (data not shown) or 129s6/SvEv (Fig. 4*B*) backgrounds. However, the proportions of

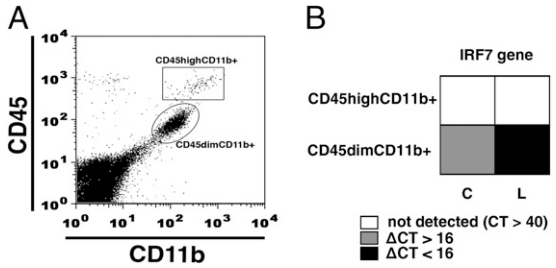

FIGURE 3. *IRF7* gene expression in FACS-sorted $CD45^{dim}Cd11b^{+}$ microglia. *A*, An example of a representative FACS profile showing the distribution of $CD45^{high}CD11b^{+}$ (macrophages) and $CD45^{dim}Cd11b^{+}$ (microglia) cell populations at 1 d postaxonal lesion. *B*, *IRF7* gene expression in $CD45^{dim}Cd11b^{+}$. ΔCT values for *IRF7* gene expression. *IRF7* gene expression could be detected in $CD45^{dim}Cd11b^{+}$ (microglia) but not in $CD45^{high}CD11b^{+}$ (macrophages) at 1 d postaxonal lesion. C, contralateral; L, lesion-reactive hippocampi.

infiltrating $CD45^{high}$ cells were significantly higher in IFNAR-KO than in WT mice (Fig. 4*B*) at 1 d. Lesion-induced increase in leukocyte infiltration in IFNAR-KO mice compared with WT was transient and was not seen at 3 and 5 d postlesion (Fig. 4*B*), although the proportion of infiltrating $CD45^{high}$ cells were increased by lesion in both WT and IFNAR-KO mice at these time (Fig. 4*B*). The fold increase in leukocyte infiltration in lesion-reactive versus contralateral hippocampus at 1 d in IFNAR-KO mice was 3-fold higher than WT (Fig. 4*C*).

Leukocyte infiltration to lesion-reactive hippocampus includes both T cells and macrophages (15, 17). To ask whether IFNAR deficiency differentially affected T cell and macrophage infiltration, we counted proportions of $CD11b^{+}$ and $TCR\text{-}\beta^{+}CD45^{high}$ cells. Whereas the proportion of macrophages ($CD45^{high}CD11b^{+}$) doubled in lesioned IFNAR-deficient hippocampus compared with WT, the lesion-induced increase in T cells ($CD45^{high}TCR\text{-}\beta^{+}$) was not affected by IFNAR deficiency (data not shown). There was no significant difference between the proportions of $CD45^{dim}CD11b^{+}$ microglia in lesion-reactive hippocampi of WT and IFNAR-KO mice (data not shown).

Lesion-induced CXCL10 *and* MMP9 *gene expression were IFNAR regulated*

Our findings indicate that IFNAR deficiency leads to increased leukocyte infiltration in lesion-reactive hippocampus. The involvement of cytokines (including TNF-α and IL-1β) and chemokines (including CCL2 and CXCL10) in leukocyte entry to CNS has been shown previously (21, 26, 27). In addition, MMPs are known to degrade extracellular matrix and to facilitate leukocyte infiltration to the CNS (28). Interestingly, type I IFN signaling regulates *MMP9* expression (29). We next examined whether increased infiltration correlated with changes in expression of lesion-induced *CCL2*, *CXCL10*, *TNF-α*, *IL-1β*, and *MMP9*. As previously shown (17, 21), axonal injury induced upregulation of *CXCL10* (Fig. 5*A*), *CCL2* (Fig. 5*B*), *TNF-α* (Fig. 5*C*), and *IL-1β* (Fig. 5*D*) in WT mice. In IFNAR-KO mice, axonal injury also induced a significant increase in *CCL2* (Fig. 5*B*), *TNF-α* (Fig. 5*C*), and *IL-1β* (Fig. 5*D*) but not in *CXCL10* gene expression (Fig. 5*A*). Unlike WT mice, *MMP9* gene expression increased significantly in lesion-reactive hippocampi from IFNAR-KO mice (Fig. 5*E*).

FJ and glial staining in response to axonal lesion

To examine whether lack of type I IFN signaling may influence axonal degeneration and glial response in the outer molecular layer of dentate gyrus, we performed FJ, Mac-1/CD11b, and GFAP staining on brain sections from WT and IFNAR-KO mice at 1, 3, and 5 d.

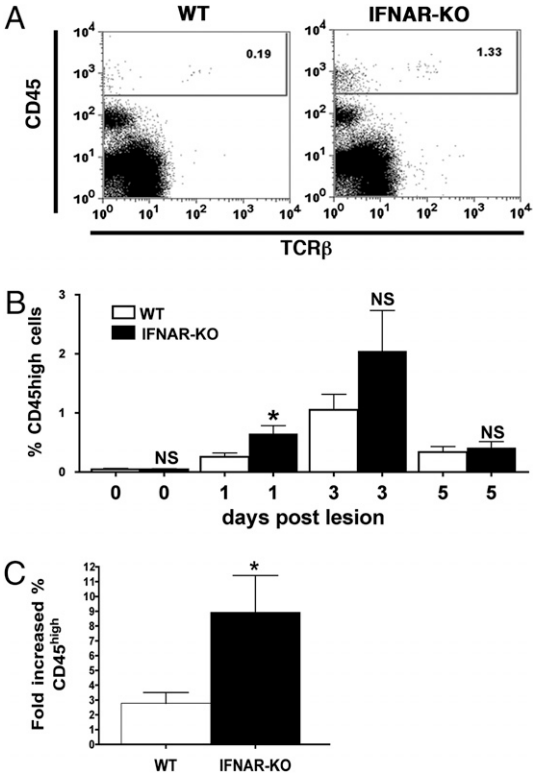

FIGURE 4. Axonal injury-induced increased leukocyte infiltration was higher in IFNAR-KO mice compared with WT mice. *A*, Representative FACS profiles for CD45 and TCR-β staining of lesion-reactive hippocampi from WT 129s6/SvEv (*left panel*) and IFNAR-KO mice on 129s6/SvEv background (*right panel*) at 1 d after axonal lesion. *B*, Lesion-induced increase in proportions of infiltrating $CD45^{high}$ cells was significantly higher in the hippocampi of 129s6/SvEv IFNAR-KO compared with WT at 1 d postlesion. However, at 0, 3, and 5 d postaxonal lesion, there was no significant difference in proportions of infiltrating $CD45^{high}$ cells in lesion-reactive hippocampi of WT compared with IFNAR-KO mice. Data were analyzed by two-tailed unpaired Student *t* test. $*p = 0.026$, day 1; statistically significant differences between lesion-reactive and WT hippocampi. *C*, The increase in leukocyte infiltration in lesion-reactive relative to contralateral hippocampus at 1 d in IFNAR-KO mice was 3-fold higher than WT. Data were analyzed by two-tailed unpaired Student *t* test; $p = 0.0085$. Error bars represent SEM. C, contralateral; L, lesion-reactive hippocampi.

FJ staining was present at a very low level in the outer molecular layer of dentate gyrus from both WT and IFNAR-KO at 1 d postaxonal lesion (Fig. 6*A*, 6*B*). The level of FJ staining increased in the outer molecular layer of dentate gyrus from both WT and IFNAR-KO at 3 (*insets* in Fig. 6*A*, 6*B*) and 5 d (data not shown) postaxonal lesion. The comparison of WT with IFNAR-KO mice showed that the lack of type I IFN signaling had no effect on FJ-staining pattern in the outer molecular layer of dentate gyrus at 1 (Fig. 6*A*, 6*B*), 3 (*insets* in Fig. 6*A*, 6*B*), and 5 d (data not shown) postlesion.

As expected, lesion caused an increase of both GFAP (Fig. 6*C*, 6*D*, arrow) and Mac-1/Cd11b (Fig. 6*E*, 6*F*, arrow) immunoreactivity in the outer molecular layer of dentate gyrus in WT at 1 (Fig. 6*C–F*), 3 (data not shown), and 5 d (data not shown). However, no differences in GFAP and Mac-1/Cd11b immunostaining were found between WT and IFNAR-deficient mice (Fig. 6*C–F*).

Discussion

Our findings show the involvement of type I IFN signaling in response to sterile injury in the CNS. Type I IFN signaling in the CNS is normally associated with antiviral immune responses (10, 30).

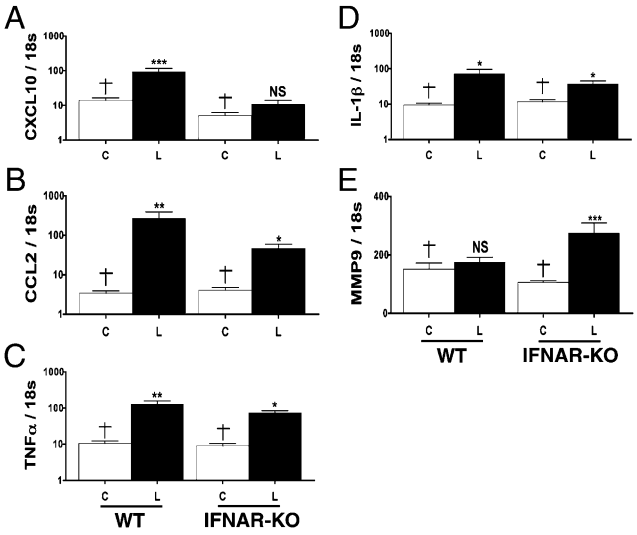

FIGURE 5. Lesion-induced *CXCL10* and *MMP9* gene expression was IFNAR dependent. Whereas *CXCL10* gene expression (*A*) did not increase significantly in lesion-reactive hippocampi of IFNAR-deficient mice, CCL2 (*B*), TNF-α (*C*), and IL-1β (*D*) were significantly increased in lesion-reactive hippocampi of both WT and IFNAR-KO mice at 1 d post-axonal lesion. (*E*) In contrast to WT, lesion induced a significant increase in *MMP9* gene expression in IFNAR-deficient mice at 1 day post axonal lesion. Data were analyzed using one-way ANOVA with Bonferroni's posthoc analysis. Error bars represent SEM. Statistically significant differences versus contralateral. $*p < 0.05$; $**p < 0.01$; $***p < 0.001$. †Not significantly different between contralaterals for each message. C, contralateral; L, lesion-reactive hippocampi.

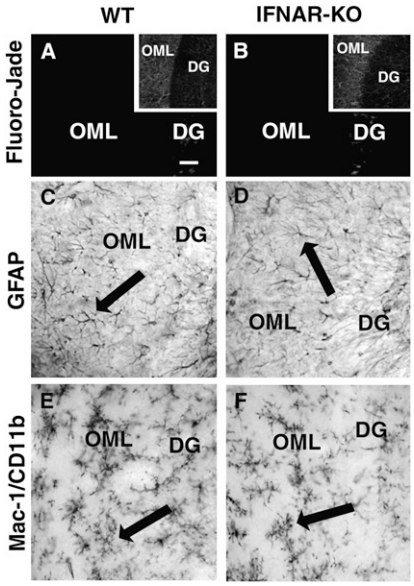

FIGURE 6. FJ, GFAP, and Mac-1/CD11b staining in the outer molecular layer of dentate gyrus in response to axonal lesion. *A* and *B*, Images showing FJ staining in lesion-reactive hippocampi of WT versus IFNAR-KO at 1 d. FJ staining was present at very low level in the outer molecular layer of dentate gyrus at 1 d postaxonal lesion. Levels of FJ staining increased in the outer molecular layer of dentate gyrus at 3 d after axonal lesion of both WT (*inset* in *A*) and IFNAR-KO (*inset* in *B*). No differences in FJ staining were observed between IFNAR-KO and WT mice. Axonal lesion caused an increase GFAP (*C*, *D*, arrows) and Mac-1/Cd11b immunoreactivity (*E*, *F*, arrows) in the outer molecular layer of dentate gyrus. However, there were no differences in GFAP and Mac-1/Cd11b immunoreactivity between IFNAR-KO and WT mice. DG, dentate gyrus; OML, outer molecular layer. Original magnification ×10 (*A*, *B*, insets), ×40 (*C*–*F*). Scale bars, 20 μm.

Type I IFNs exert a wide range of effects on inflammatory processes in the CNS during infection and in EAE, in both of which pathogen-associated signals may play a role. The functional significance of type I IFN in sterile injury-induced response in the CNS is therefore of interest. Similar to findings in viral infection models (10, 30), the expression of *IRF7* and *IRF9* gene increased following axonal lesion, and this increase was IFNAR dependent (10). Other studies have shown a role for type I IFN in regulating leukocyte infiltration to the CNS in EAE models (11, 12, 31), and we have shown a similar effect in response to sterile injury. Our results support an innate signaling role for type I IFN in the CNS.

IRF7 and IRF9 belong to a family of transcription factors with diverse functions including host defense, regulation of cell growth, apoptosis, and immune cell development. However, mice deficient in IRF7 and IRF9 develop normally and have no obvious differences in size and behavior compared with WT littermates (9, 32). Most importantly, these two reports emphasize the essential role of IRF7 and IRF9 in the regulation of type I IFN signaling and antiviral defense. The CNS is susceptible to infection, and constitutive expression of IRF7 and IRF9 may therefore be necessary for initiation of type I IFN response to infection. In the current study, we showed CNS upregulation of IRF7 and IRF9 in response to injury, which suggest their involvement in noninfectious responses as well.

IRF7 gene expression is specifically of interest, because it positively regulates the induction of type I IFN, which in turn regulates *IRF7* induction. The cellular expression of *IRF7* may therefore be indicative of the source of type I IFN. We have been able to show induction of IFN-α and IFN-β by RT-PCR in lesion-reactive hippocampus, but this has been difficult to reproduce, and we have been unable to localize the cellular source of IFN I. This is probably due to a combination of low expression level and that current methods are not sensitive enough to detect the differences in type I IFN induced by injury in this model. Identification and localization of type I IFN in the CNS is of interest, particularly in response to viral infection. To our knowledge, only two studies have identified the source of type I IFN in the CNS. Delhaye et al. (30) identified that neurons produced IFN-α in response to infection, and Teige et al. (12) found that during EAE, both infiltrating cells and cells with the morphology of microglia expressed IFN-β. Otherwise, surrogate markers of downstream signaling associated with type I IFN signaling have been used to identify type I IFN-producing cells within the CNS (10, 30).

Our results pointed to upregulation of IRF7 in Mac-1/CD11b$^+$ microglia/macrophages, although absence of IRF7 immunoreactivity in other cell types does not exclude their ability to produce type I IFN. IRF7 protein expression could be detected in unmanipulated hippocampal samples as well as in contralateral and lesion-reactive hippocampi. Furthermore, both PCR and Western blot analysis showed that the level of IRF7 protein expression was higher in WT mice compared with IFNAR-KO mice, although not significantly. The immunostaining of sections with IRF7 Ab showed increased but dispersed IRF7$^+$ cells in the outer molecular layer of dentate gyrus in response to axonal lesion. This increased immunoreactivity was not detected by Western blotting, which probably reflects lower sensitivity of Western blotting of whole hippocampal isolates versus immunohistochemistry, by which IRF7 expression could be detected even in very few cells.

We showed that the axonal lesion resulted in increased expression of *IRF7* gene, and this increase was IFNAR dependent. IFNAR-dependent induction of *IRF7* has also been shown in

response to toxin-induced demyelination, although there appeared to be no role for type I IFN signaling, and the cell source was not identified (33). In virally infected brain, *IRF7* gene expression was detected in astrocytes, microglia, neurons, and infiltrating $CD3^+$ T cells (10). Another study showed that viral infection induced upregulation of IRF7 and type I IFN in neurons as well as in Mac-1/$CD11b^+$ microglia/macrophages (30). It is also evident that all cells in the CNS can respond to type I IFN (30, 34–36). *IRF7* alone or together with IRF3 can induce transcription of type I IFN (8, 25). Hippocampal *IRF3* gene expression was unaltered in response to axonal lesion in both WT and IFNAR-KO after 1 d, suggesting that IRF3 may not be involved in this case. Similarly, viral infection in the CNS did not induce changes in *IRF3* gene expression, even after several days (10).

Our findings extend to the sterile injury response observation of type I IFN regulation of leukocyte entry to the CNS. The proportion of $CD45^{high}CD11b^+$ macrophages but not of $CD45^{high}TCR\text{-}\beta^+$ T cells doubled in IFNAR-KO in comparison with WT animals at 1 d postaxonal lesion. Analogous effects of type I IFN signaling on infiltration of macrophages to the CNS have been demonstrated in EAE (11, 12, 31). Increased clinical scores of EAE in IFNAR-KO mice were associated with elevated number of MAC-3^+ macrophages (11), and treatment with IFN-β reduced both the clinical scores and the number of $ED1^+$ macrophages in rats (31). In addition, it was reported that the CNS of IFN-β–KO mice contained more activated macrophages than in WT mice (12). Lack of type I IFN signaling had no effect on T cell infiltration in the two of these studies, in which it was examined (11, 12).

Unlike in WT mice, *CXCL10* gene expression was not elevated in lesioned IFNAR-KO mice. In contrast, CCL2, TNF-α, and IL-1β were similarly upregulated in both IFNAR-KO and WT mice. This contrasts with findings in EAE, in which elevated macrophage infiltration correlated with increased levels of TNF-α, CCL2, and *CXCL10* expression in IFNAR- and IFN-β–KO compared with WT mice (11, 12). As shown by others and ourselves in entorhinal cortex lesion and other models of brain injury, glial cells represent a major source for many of these mediators. Previous studies identified microglia and astrocytes as a prominent source of CCL2 (17). IL-1β and TNF are also glial derived (37, 38), and we must assume that the leukocyte contribution was not significant in this case. The differences in effect on *CXCL10* may reflect involvement of adjuvant in the EAE model or other differences between these systems. It has been demonstrated that an IFN-stimulated response element is contained in the *CXCL10* promoter (39, 40). Type I IFN is capable of stimulating *CXCL10* production by hepatocytes in vitro, and ischemia/reperfusion-triggered intrahepatic *CXCL10* expression was diminished in IFNAR-KO mice (41). The induction of *CXCL10* has been used as biomarker to measure type I IFN activity (42). Our study suggests that type I IFN signaling normally either allows or directly stimulates CXCL10 production in the CNS in response to axonal injury. Our findings further suggest that type I IFN signaling may regulate leukocyte entry through this or other mechanisms involving disruption of blood-brain barrier (29). MMP9 is involved in degradation of extracellular matrix and facilitating the recruitment of leukocytes (28, 43). In the CNS, both astrocytes and microglia express *MMP9* (28), and it is also expressed by infiltrating macrophages (44). It has been shown that type I IFN inhibits *MMP9* expression in astrocytes and microglia and reduces leukocyte infiltration to the CNS (29, 43, 45–47). We find that in the absence of type I IFN signaling, *MMP9* was significantly increased. This could both result from and contribute to the increased leukocyte entry into the hippocampus of IFNAR-deficient mice in response to axonal lesion.

These findings of innate expression and response to type I IFN in the CNS likely have relevance to understanding the effectiveness of IFN-β as a therapeutic for multiple sclerosis. Innate signaling pathways in the CNS offer potential new targets for therapy for neuroinflammatory diseases.

Acknowledgments

We thank Dina Draeby, Mie Rytz Hansen, and Pia Nyborg Nielsen for excellent technical support. We also thank Dr. Alicia Babcock for providing RNA samples used in preliminary studies. We thank Per Svenningsen for help with the confocal laser microscopy and Inger Andersen for help with cell sorting.

Disclosures

The authors have no financial conflicts of interest.

References

1. Jones, T. B., E. E. McDaniel, and P. G. Popovich. 2005. Inflammatory-mediated injury and repair in the traumatically injured spinal cord. *Curr. Pharm. Des.* 11: 1223–1236.
2. Schwartz, M. 2003. Macrophages and microglia in central nervous system injury: are they helpful or harmful? *J. Cereb. Blood Flow Metab.* 23: 385–394.
3. Pineau, I., and S. Lacroix. 2009. Endogenous signals initiating inflammation in the injured nervous system. *Glia* 57: 351–361.
4. Larsen, P. H., T. H. Holm, and T. Owens. 2007. Toll-like receptors in brain development and homeostasis. *Sci. STKE* 2007: pe47.
5. Theofilopoulos, A. N., R. Baccala, B. Beutler, and D. H. Kono. 2005. Type I interferons (α/β) in immunity and autoimmunity. *Annu. Rev. Immunol.* 23: 307–336.
6. Prakash, A., E. Smith, C. K. Lee, and D. E. Levy. 2005. Tissue-specific positive feedback requirements for production of type I interferon following virus infection. *J. Biol. Chem.* 280: 18651–18657.
7. Schindler, C., D. E. Levy, and T. Decker. 2007. JAK-STAT signaling: from interferons to cytokines. *J. Biol. Chem.* 282: 20059–20063.
8. Honda, K., H. Yanai, A. Takaoka, and T. Taniguchi. 2005. Regulation of the type I IFN induction: a current view. *Int. Immunol.* 17: 1367–1378.
9. Honda, K., H. Yanai, H. Negishi, M. Asagiri, M. Sato, T. Mizutani, N. Shimada, Y. Ohba, A. Takaoka, N. Yoshida, and T. Taniguchi. 2005. IRF-7 is the master regulator of type-I interferon-dependent immune responses. *Nature* 434: 772–777.
10. Ousman, S. S., J. Wang, and I. L. Campbell. 2005. Differential regulation of interferon regulatory factor (IRF)-7 and IRF-9 gene expression in the central nervous system during viral infection. *J. Virol.* 79: 7514–7527.
11. Prinz, M., H. Schmidt, A. Mildner, K. P. Knobeloch, U. K. Hanisch, J. Raasch, D. Merkler, C. Detje, I. Gutcher, J. Mages, et al. 2008. Distinct and nonredundant in vivo functions of IFNAR on myeloid cells limit autoimmunity in the central nervous system. *Immunity* 28: 675–686.
12. Teige, I., A. Treschow, A. Teige, R. Mattsson, V. Navikas, T. Leanderson, R. Holmdahl, and S. Issazadeh-Navikas. 2003. IFN-β gene deletion leads to augmented and chronic demyelinating experimental autoimmune encephalomyelitis. *J. Immunol.* 170: 4776–4784.
13. Finsen, B., M. B. Jensen, N. D. Lomholt, I. V. Hegelund, F. R. Poulsen, and T. Owens. 1999. Axotomy-induced glial reactions in normal and cytokine transgenic mice. *Adv. Exp. Med. Biol.* 468: 157–171.
14. Ladeby, R., M. Wirenfeldt, I. Dalmau, R. Gregersen, D. García-Ovejero, A. Babcock, T. Owens, and B. Finsen. 2005. Proliferating resident microglia express the stem cell antigen CD34 in response to acute neural injury. *Glia* 50: 121–131.
15. Babcock, A. A., M. Wirenfeldt, T. Holm, H. H. Nielsen, L. Dissing-Olesen, H. Toft-Hansen, J. M. Millward, R. Landmann, S. Rivest, B. Finsen, and T. Owens. 2006. Toll-like receptor 2 signaling in response to brain injury: an innate bridge to neuroinflammation. *J. Neurosci.* 26: 12826–12837.
16. Wirenfeldt, M., L. Dissing-Olesen, A. Anne Babcock, M. Nielsen, M. Meldgaard, J. Zimmer, I. Azcoitia, R. G. Leslie, F. Dagnaes-Hansen, and B. Finsen. 2007. Population control of resident and immigrant microglia by mitosis and apoptosis. *Am. J. Pathol.* 171: 617–631.
17. Babcock, A. A., W. A. Kuziel, S. Rivest, and T. Owens. 2003. Chemokine expression by glial cells directs leukocytes to sites of axonal injury in the CNS. *J. Neurosci.* 23: 7922–7930.
18. Fagan, A. M., and F. H. Gage. 1994. Mechanisms of sprouting in the adult central nervous system: cellular responses in areas of terminal degeneration and reinnervation in the rat hippocampus. *Neuroscience* 58: 705–725.
19. Frotscher, M., B. Heimrich, and T. Deller. 1997. Sprouting in the hippocampus is layer-specific. *Trends Neurosci.* 20: 218–223.
20. Savaskan, N. E., and R. Nitsch. 2001. Molecules involved in reactive sprouting in the hippocampus. *Rev. Neurosci.* 12: 195–215.
21. Khorooshi, R., A. A. Babcock, and T. Owens. 2008. NF-κB-driven STAT2 and CCL2 expression in astrocytes in response to brain injury. *J. Immunol.* 181: 7284–7291.

22. Babcock, A. A., H. Toft-Hansen, and T. Owens. 2008. Signaling through MyD88 regulates leukocyte recruitment after brain injury. *J. Immunol.* 181: 6481–6490.
23. Meraz, M. A., J. M. White, K. C. Sheehan, E. A. Bach, S. J. Rodig, A. S. Dighe, D. H. Kaplan, J. K. Riley, A. C. Greenlund, D. Campbell, et al. 1996. Targeted disruption of the Stat1 gene in mice reveals unexpected physiologic specificity in the JAK-STAT signaling pathway. *Cell* 84: 431–442.
24. Schmued, L. C., C. C. Stowers, A. C. Scallet, and L. Xu. 2005. Fluoro-Jade C results in ultra high resolution and contrast labeling of degenerating neurons. *Brain Res.* 1035: 24–31.
25. Seth, R. B., L. Sun, and Z. J. Chen. 2006. Antiviral innate immunity pathways. *Cell Res.* 16: 141–147.
26. Sedgwick, J. D., D. S. Riminton, J. G. Cyster, and H. Körner. 2000. Tumor necrosis factor: a master-regulator of leukocyte movement. *Immunol. Today* 21: 110–113.
27. Babcock, A., and T. Owens. 2003. Chemokines in experimental autoimmune encephalomyelitis and multiple sclerosis. *Adv. Exp. Med. Biol.* 520: 120–132.
28. Agrawal, S. M., L. Lau, and V. W. Yong. 2008. MMPs in the central nervous system: where the good guys go bad. *Semin. Cell Dev. Biol.* 19: 42–51.
29. Benveniste, E. N., and H. Qin. 2007. Type I interferons as anti-inflammatory mediators. *Sci. STKE* 2007: pe70.
30. Delhaye, S., S. Paul, G. Blakqori, M. Minet, F. Weber, P. Staeheli, and T. Michiels. 2006. Neurons produce type I interferon during viral encephalitis. *Proc. Natl. Acad. Sci. USA* 103: 7835–7840.
31. Floris, S., S. R. Ruuls, A. Wierinckx, S. M. van der Pol, E. Döpp, P. H. van der Meide, C. D. Dijkstra, and H. E. De Vries. 2002. Interferon-β directly influences monocyte infiltration into the central nervous system. *J. Neuroimmunol.* 127: 69–79.
32. Kimura, T., Y. Kadokawa, H. Harada, M. Matsumoto, M. Sato, Y. Kashiwazaki, M. Tarutani, R. S. Tan, T. Takasugi, T. Matsuyama, et al. 1996. Essential and non-redundant roles of p48 (ISGF3 γ) and IRF-1 in both type I and type II interferon responses, as revealed by gene targeting studies. *Genes Cells* 1: 115–124.
33. Schmidt, H., J. Raasch, D. Merkler, F. Klinker, S. Krauss, W. Brück, and M. Prinz. 2009. Type I interferon receptor signalling is induced during demyelination while its function for myelin damage and repair is redundant. *Exp. Neurol.* 216: 306–311.
34. Okada, K., E. Kuroda, Y. Yoshida, U. Yamashita, A. Suzumura, and S. Tsuji. 2005. Effects of interferon-β on the cytokine production of astrocytes. *J. Neuroimmunol.* 159: 48–54.
35. Njenga, M. K., L. R. Pease, P. Wettstein, T. Mak, and M. Rodriguez. 1997. Interferon α/β mediates early virus-induced expression of H-2D and H-2K in the central nervous system. *Lab. Invest.* 77: 71–84.
36. Heine, S., J. Ebnet, S. Maysami, and M. Stangel. 2006. Effects of interferon-β on oligodendroglial cells. *J. Neuroimmunol.* 177: 173–180.
37. Clausen, B. H., K. L. Lambertsen, A. A. Babcock, T. H. Holm, F. Dagnaes-Hansen, and B. Finsen. 2008. Interleukin-1β and tumor necrosis factor-α are expressed by different subsets of microglia and macrophages after ischemic stroke in mice. *J. Neuroinflammation* 5: 46.
38. Jensen, M. B., I. V. Hegelund, N. D. Lomholt, B. Finsen, and T. Owens. 2000. IFNγ enhances microglial reactions to hippocampal axonal degeneration. *J. Neurosci.* 20: 3612–3621.
39. Majumder, S., L. Z. Zhou, P. Chaturvedi, G. Babcock, S. Aras, and R. M. Ransohoff. 1998. p48/STAT-1α-containing complexes play a predominant role in induction of IFN-γ–inducible protein, 10 kDa (IP-10) by IFN-γ alone or in synergy with TNF-α. *J. Immunol.* 161: 4736–4744.
40. Wu, C., Y. Ohmori, S. Bandyopadhyay, G. Sen, and T. Hamilton. 1994. Interferon-stimulated response element and NF κB sites cooperate to regulate double-stranded RNA-induced transcription of the IP-10 gene. *J. Interferon Res.* 14: 357–363.
41. Zhai, Y., B. Qiao, F. Gao, X. Shen, A. Vardanian, R. W. Busuttil, and J. W. Kupiec-Weglinski. 2008. Type I, but not type II, interferon is critical in liver injury induced after ischemia and reperfusion. *Hepatology* 47: 199–206.
42. Petry, H., L. Cashion, P. Szymanski, O. Ast, A. Orme, C. Gross, M. Bauzon, A. Brooks, C. Schaefer, H. Gibson, et al. 2006. Mx1 and IP-10: biomarkers to measure IFN-β activity in mice following gene-based delivery. *J. Interferon Cytokine Res.* 26: 699–705.
43. Stuve, O., S. Chabot, S. S. Jung, G. Williams, and V. W. Yong. 1997. Chemokine-enhanced migration of human peripheral blood mononuclear cells is antagonized by interferon β-1b through an effect on matrix metalloproteinase-9. *J. Neuroimmunol.* 80: 38–46.
44. Agrawal, S., P. Anderson, M. Durbeej, N. van Rooijen, F. Ivars, G. Opdenakker, and L. M. Sorokin. 2006. Dystroglycan is selectively cleaved at the parenchymal basement membrane at sites of leukocyte extravasation in experimental autoimmune encephalomyelitis. *J. Exp. Med.* 203: 1007–1019.
45. Veldhuis, W. B., J. W. Derksen, S. Floris, P. H. Van Der Meide, H. E. De Vries, J. Schepers, I. M. Vos, C. D. Dijkstra, L. J. Kappelle, K. Nicolay, and P. R. Bär. 2003. Interferon-β blocks infiltration of inflammatory cells and reduces infarct volume after ischemic stroke in the rat. *J. Cereb. Blood Flow Metab.* 23: 1029–1039.
46. Veldhuis, W. B., S. Floris, P. H. van der Meide, I. M. Vos, H. E. de Vries, C. D. Dijkstra, P. R. Bär, and K. Nicolay. 2003. Interferon-β prevents cytokine-induced neutrophil infiltration and attenuates blood-brain barrier disruption. *J. Cereb. Blood Flow Metab.* 23: 1060–1069.
47. Liuzzi, G. M., T. Latronico, A. Fasano, G. Carlone, and P. Riccio. 2004. Interferon-β inhibits the expression of metalloproteinases in rat glial cell cultures: implications for multiple sclerosis pathogenesis and treatment. *Mult. Scler.* 10: 290–297.